Published in final edited form as:
Clin Cancer Res. 2010 July 15; 16(14): 3639–3647. doi:10.1158/1078-0432.CCR-09-3385.

Augmentation of radiation response by motesanib, a multikinase inhibitor that targets vascular endothelial growth factor receptors

Tim J. Kruser[1], **Deric L. Wheeler**[1], **Eric A. Armstrong**[1], **Mari Iida**[1], **Kevin R. Kozak**[1], **Albert J. van der Kogel**[2], **Johan Bussink**[2], **Angela Coxon**[3], **Anthony Polverino**[3], and **Paul M. Harari**[1]

[1]Department of Human Oncology, Paul P. Carbone Comprehensive Cancer Center, University of Wisconsin School of Medicine & Public Health [2]Department of Radiation Oncology, Radboud University Nijmegen Medical Centre, Nijmegen, the Netherlands [3]Department of Oncology Research, Amgen Inc., Thousand Oaks, CA

Abstract

Background—Motesanib is a potent inhibitor of VEGFR1, 2 and 3, PDGFR and Kit receptors. In this report we examine the interaction between motesanib and radiation *in vitro* and in head and neck squamous cell carcinoma (HNSCC) xenograft models.

Experimental Design—*In vitro* assays were performed to assess the impact of motesanib on VEGFR2 signaling pathways in human umbilical vein endothelial cells (HUVECs). HNSCC lines grown as tumor xenografts in athymic nude mice were utilized to assess the *in vivo* activity of motesanib alone and in combination with radiation.

Results—Motesanib inhibited VEGF-stimulated HUVEC proliferation *in vitro*, as well as VEGFR2 kinase activity. Additionally motesanib and fractionated radiation showed additive inhibitory effects on HUVEC proliferation. *In vivo* combination therapy with motesanib and radiation showed increased response compared to drug or radiation alone in UM-SCC1 ($p<0.002$) and SCC-1483 xenografts ($p=0.001$); however the combination was not significantly more efficacious than radiation alone in UM-SCC6 xenografts. Xenografts treated with motesanib demonstrated a reduction of vessel penetration into tumor parenchyma, compared to control tumors. Furthermore, triple immunohistochemical staining for vasculature, proliferation, and hypoxia demonstrated well-defined spatial relationships between these parameters in HNSCC xenografts. Motesanib significantly enhanced intratumoral hypoxia in the presence and absence of fractionated radiation.

Conclusions—These studies identify a favorable interaction when combining radiation and motesanib in HNSCC models. Data presented suggest that motesanib reduces blood vessel penetration into tumors and thereby increases intratumoral hypoxia. These findings suggest that clinical investigations examining combinations of radiation and motesanib are warranted in HNSCC.

Reprint requests: Paul M. Harari, Box 3684 Clinical Science Center-K4/B100, 600 Highland Avenue, Madison, WI 53792. Phone: (608) 263-5009; Fax: (608) 262-6126;, harari@humonc.wisc.edu.

Conflict of Interest Notification: AC and AP are employees of Amgen, Inc.

PMH and KRK hold laboratory research agreements with Amgen, Inc.

Introduction

Head and neck squamous cell carcinoma (HNSCC) is the sixth most common cancer worldwide with a global yearly incidence of over 500,000 new cases (1). Despite stepwise advances associated with combinations of radiation and chemotherapy (2), only 30–50% of advanced stage patients are cured of their disease. Therefore molecularly targeted agents are under investigation in conjunction with radiation and/or chemoradiation in HNSCC. A recent international phase III trial that combined the anti-EGFR monoclonal antibody cetuximab with radiation in HNSCC patients demonstrated a near doubling of median survival for patients receiving the EGFR inhibitor (3). Furthermore, the addition of cetuximab to radiation did not appear to augment radiation-induced toxicities. This study highlighted the potential of targeted agents in HNSCC patients undergoing curative radiation; additional novel treatments are highly desired.

Targeting the vascular endothelial growth factor (VEGF) receptor has drawn interest in HNSCC. VEGF is a potent mitogen for vascular endothelial cells and acts through specific tyrosine kinase receptors – VEGFR1 (Flt-1), VEGFR2 (Flk-1) and VEGFR3 (Flt-3). As tumors enlarge, neovascularization becomes necessary for growth and metastasis. Strong evidence demonstrates that VEGFR signaling is an important pathway in tumors of the upper aerodigestive tract, including HNSCC (4–6). Additionally, tumor levels of VEGF have been shown to predict poor prognosis in numerous solid malignancies.

VEGF signaling is thought to play a role in radioresistance (7, 8). VEGF expression is influenced by hypoxia-inducible factor 1α (HIF1α); therefore the microregional distribution of hypoxia can influence tumor radioresistance and proliferation via VEGF pathways (9). Additionally, evidence suggests that radiation upregulates platelet-derived growth factor receptor (PDGFR) signaling in endothelial cells, which may contribute to radiation resistance (10). Motesanib is a potent inhibitor of the VEGFR1/Flt1, VEGFR2/Flk-1, VEGFR3/Flt3, PDGFR, and Kit receptors in preclinical models (11). It has been demonstrated to inhibit these receptors in the nanomolar range, but shows little activity against kinases such as the epidermal growth factor receptor (EGFR), Src, and the fibroblast growth factor (FGF) receptor. Motesanib has undergone testing in patients with advanced, refractory solid tumors with encouraging preliminary results (12). However, the interaction between motesanib and radiation has not been characterized. In this study we demonstrate enhanced anti-tumor effect when combining radiation with motesanib in HNSCC xenograft models, and present evidence that alterations in the tumor microenvironment accompany this observed interaction.

Materials and Methods

Cell lines and compounds

Human HNSCC lines UM-SCC1 and UM-SCC6 were provided by Dr. Thomas E. Carey (University of Michigan, Ann Arbor, MI) and SCC-1483 cells were provided by Dr. Jennifer Grandis (University of Pittsburgh, Pittsburgh, PA). SCC cells were cultured in DMEM supplemented with 10% fetal bovine serum (FBS), 1 μg/ml hydrocortisone, and 1% penicillin/streptomycin. SCC cell culture media and supplements were obtained from Invitrogen (Carlsbad, CA). Human umbilical vein endothelial cells (HUVECs) were purchased from ATCC (Manassas, VA). HUVECs were cultured in endothelial basal medium-2 (EBM-2) supplemented with EGM-2 SingleQuots growth supplements (Lonza, Basel, Switzerland) and 1% penicillin/streptomycin.

Immunoprecipitation and immunoblotting

HUVECs were grown to 70% confluence and treated with either motesanib or dimethyl sulfoxide (DMSO) vehicle control for 24 hours. Final concentration in all plates of DMSO was 0.25%. Cells were exposed to either 50 ng/ml VEGF or vehicle for 45 minutes, and then whole cell lysates were obtained using Tween-20 lysis buffer. Immunoprecipitation of VEGFR2 was performed by incubating 700 ug of HUVEC lysate with 1.5 ug of rabbit anti-FLK-1 (sc-504, SantaCruz Biotechnology (SCB) Inc., Santa Cruz CA). After adding 30μl of protein A/G agarose beads (sc-2003, SCB), lysates were incubated for another 2 hours at 4°C. The immunoprecipitates were pelleted by centrifugation and washed three times with Tween-20 lysis buffer. The captured immune-complexes were then eluted by boiling the beads in 2xSDS sample buffer for 5 minutes and subjected to gel electrophoresis and transfer to Immobilon-P membrane (Millipore, Billerica, MA). Primary antibody for western blot detection of VEGFR2 was murine anti-Flk-1 (sc-6251, SCB); primary pTyr antibody was murine anti-pTyr antibody (#05-321, Upstate, Lake Placid NY). Secondary antibody for detection was HRP-conjugated goat-anti-mouse IgG (sc-2005, SCB). Thereafter, proteins were detected via enhanced chemiluminescence (ECL+) detection system (Amersham Biosciences, Piscataway, NJ).

VEGFR kinase assay

VEGFR-2 kinase activity was quantified in the presence of serial dilutions of motesanib using the HTScan VEGF Receptor 2 Kinase Assay Kit according to manufacturer's instructions (Cell Signaling, Danvers, MA).

HUVEC proliferation assays

Crystal violet assay—Cells were grown in EBM-2 basal medium with 2% FBS, without exogenous growth factors (i.e. EGM-2 SingleQuots growth supplements were omitted). VEGF stimulation was 25 ng/ml every 24 hours x 4 days. Final DMSO concentration was 0.25% in all wells. Data points represented as the mean crystal violet staining intensity (6 wells per condition) +/− SEM.

HUVEC counting after motesanib and radiation—HUVECs were plated at a density of 15,000 cells per p100 dish (27 dishes) at day 0. At day one, three dishes were rinsed with PBS/0.02 % EDTA, detached using 0.05% Trypsin/EDTA, and counted via trypan blue exclusion to establish a baseline number of cells/plate for the cohort. The remaining plates were treated with either motesanib (25 nM) or vehicle control and three hours later half of the plates were irradiated at 2 Gy with a Shepherd & Associates Model 109 irradiator (San Fernando, CA) and a ^{137}cesium hotbox source. On day 3 the HUVECs on half of the plates were trypsinized and counted; the other half received fresh media +/− motesanib and 2 Gy radiation where indicated. The remaining HUVEC plates were trypsinized and counted at day 4 to establish the final data points.

Tumor growth in athymic nude mice

Athymic nude mice (3–4-week-old males) were obtained from Harlan Bioproducts for Science (Indianapolis, IN). The care and treatment of experimental animals was in accordance with institutional guidelines. Cells (~2 x 10^6) from the respective human cancer lines were injected subcutaneously into the flank area on day 0. Tumor volume was determined by direct measurement with calipers and calculated by the formula (π)/6 x (large diameter) x (small diameter)^2. Motesanib or vehicle control was administered once daily by oral gavage at specified doses five days per week. Motesanib doses were chosen based on pilot experiments testing the *in vivo* efficacy of motesanib alone in the respective xenografts. Radiation treatment was delivered via a Philips RT-250 orthovoltage unit (Philips Medical

Systems, Bothell, WA) using custom-designed mouse jigs, which specifically exposed the dorsal flank (harboring tumor xenografts) for irradiation.

Immunohistochemistry

Mice harboring UM-SCC1 xenografts were treated with vehicle control, motesanib, fractionated radiation, or the combination (see "Tumor Growth" above for details), and harvested 3 hours after the last treatment for IHC examination.

Von Willebrand Factor (vWF)—vWF expression was detected in histologic sections of tumor xenografts. Briefly, excised tumor specimens were fixed in 10% neutral buffered formalin. Following embedding in paraffin, 5-μm sections were cut, and tissue sections were mounted. Sections were dried, deparaffinized, and rehydrated. vWF antigen was unmasked with Proteinase K at 37°C for 20 min. After quenching endogenous peroxidase activity and blocking nonspecific binding sites, slides were incubated at 4°C overnight with primary antibody (vWF, 1/150 Dako, Carpinteria, CA) followed by a 30-min incubation of secondary antibody. Slides then were incubated with streptavidin peroxidase, visualized using the 3,3'-diaminobenzidine chromogen (Lab Vision Corp, Fremont, CA), counterstained with hematoxylin, dehydrated, and mounted. Quantitative analysis was performed for the results of immunohistochemical examination by assessing the numbers of vessels per high-powered field (HPF), as well as the proportion of vWF expression at x100 magnification. Five HPFs were randomly chosen and examined from each of vehicle and MSB tumor (n=2 tumors per group), and vessels per HPF were counted. Percentage of vWF immunoreactive area was measured by Image J software. Statistical significance was analyzed by Student's t-test.

Hypoxia (Pimonidazole), proliferation (Ki67), and vasculature (9F1)—One hour after administration of the final radiation dose, three mice per treatment group received 60 mg/kg of pimonidazole HCl (Hydroxyprobe™-1, NPI, Inc., Burlington, MA) via intraperitoneal injection. Two hours later the mice were euthanized, and tumors were excised and frozen. To minimize fracturing of tumor specimens during freezing, no embedding medium was used, and tumors were slowly frozen by placing them in small plastic boats floating in a mixture of isopentane and dry ice. The tissues were then wrapped in dry ice-chilled foil to minimize desiccation, and packaged in dry ice. Frozen sections (5 μm) were fixed in acetone (4 C), and the Hoechst 33342 signal was recorded on air-dried tissue sections. After re-hydration, tumor sections were triple-stained for pimonidazole, vasculature and Ki67.

Ki67 was visualized with rabbit anti-Ki67 (Calbiochem, San Diego CA) and goat anti-rabbitFabCy3 (Jackson Immuno Research). In the same tissue section pimonidazole was detected with a polyclonal rabbit-anti-pimonidazole and donkey-anti-rabbit F(ab')2Alexa488 (Molecular Probes, Eugene, Oregon). Finally, again in the same section blood vessels were visualized using undiluted 9F1 supernatant, a rat monoclonal antibody to mouse endothelium (to phosphotyrosine), (Department of Pathology, Radboud University Nijmegen Medical Centre, Nijmegen, The Netherlands)) and chicken-anti-rat ALEXA647 (Molecular Probes).

Image acquisition, processing, and analysis

The tumor-sections were mounted with Fluorostab (Euro Diagnostica) and quantitatively analyzed with a semi-automatic image recording system as previously described (13). Using different filter sets, multiple scans at 100x magnification yielded composite images of hypoxia (pimonidazole), proliferation (Ki67) and vasculature (9F1). The gray scale images were thresholded into binary images, which were used for quantitative analysis of the

vasculature, hypoxia, and proliferative labeling indices. A consecutive H&E stained tumor section was used to define the tumor area excluding non-tumor tissue, necrosis and staining artifacts.

Results

Motesanib has specific activity on HUVECs *in vitro*

In the absence of VEGF (HUVECs grown in basal medium with 2% FBS, without exogenous growth factors) motesanib showed no significant antiproliferative effect on HUVECs; however, in the presence of VEGF stimulation, motesanib inhibited the pro-mitogenic effect of VEGF in a dose-dependent manner (Fig. 1A). These dose-dependent anti-proliferative observations are mirrored by the ability of motesanib to block both the VEGF-stimulated kinase activity of VEGFR2 (Fig 1B), as well as VEGF-stimulated phosphorylation of VEGFR2 (Fig 1C). The nanomolar range of activity of motesanib observed is in line with previous studies (11).

To examine the effect of motesanib in combination with radiation on HUVEC proliferation *in vitro*, HUVECs were grown in medium fully supplemented with exogenous growth factors, including VEGF. Motesanib demonstrated minimal antiproliferative activity on cell growth alone, while fractionated radiation significantly reduced the number of HUVECs present after four days of stimulation (Fig. 1D). The combination of motesanib and fractionated radiation showed an additive inhibition on HUVEC proliferation at the p=0.08 level, 2-sided t-test. Expression of VEGFR1, VEGFR2, VEGFR3, PDGFR and c-Kit were not detectable by western blot analysis in any of the HNSCC tumor lines tested (Supplemental Figure 1), and motesanib had no activity on HNSCC cells *in vitro* using either proliferative assays or clonogenic radiation assays (data not shown).

Motesanib augments *in vivo* radiation response

To investigate the effects of combining motesanib and radiation *in vivo*, mice bearing established HNSCC xenografts were treated with vehicle control, radiation alone, motesanib alone, or radiation and motesanib combined. Treatment was initiated approximately 19–23 days post implantation of cells once tumors had established. Mouse weights were measured weekly, and no discernible toxicity was observed in motesanib-treated groups.

In UM-SCC1 xenografts measured 24 days after initiation of treatment, motesanib 75 mg/kg QD alone resulted in a 15% reduction in tumor volume as compared to control tumors (Fig. 2A); however this was not significant (p=0.38). Low dose radiation alone resulted in a 45% reduction in tumor volumes (p<0.01). The combination of radiation and motesanib resulted in a 72% growth reduction (p=0.0001); this effect was significantly larger than that observed with either motesanib alone (p=0.0001) or radiation alone (p<0.002).

In SCC-1483 xenografts measured 21 days after initiation of treatment, motesanib 75 mg/kg daily alone resulted in a 46% reduction in tumor volume (p< 0.02) (Fig. 2B). Treatment of xenografts with radiation alone resulted in a 43% reduction (p=0.004) in tumor volume while the combination of radiation and motesanib resulted in a 72% reduction in tumor volume when compared to drug alone (p<0.0001). The combination of radiation and motesanib resulted in more pronounced tumor growth inhibition than either motesanib alone (p=0.008) or radiation alone (p=0.001).

In UM-SCC6 xenografts, motesanib 20 mg/kg daily alone resulted in a reduction in tumor volume (Fig. 2C); however this was not statistically significant. The combination of motesanib and radiation resulted in more pronounced tumor growth inhibition than

motesanib alone (p=0.01 at day 50), but the combined effect was not significantly greater than radiation alone in terms of antitumor effect.

Motesanib and radiation alter xenograft histomorphology

To examine the effect of combining radiation and motesanib on tumor tissue, we performed immunohistochemistical analyses to examine tumor vascularity and architecture. UM-SCC1 xenografts treated with vehicle control, radiation, motesanib, or the combination were harvested three hours after the last radiation treatment (as indicated in Fig. 2A). Tissue was fixed and stained for vWF, which is constitutively expressed in endothelium. Vehicle-treated tumors demonstrate large areas of viable tumor cells with prominent vessels coursing through tumor parenchyma (Fig. 3A). To examine the effect of motesanib on tumor vasculature, we analyzed the vessels per high-powered field (HPF), as well as the proportion of tumor area staining positive for vWF. Motesanib treatment (75 mg/kg x 4 weeks) reduced the number of vessels per HPF (6.3±1.4 vs 3.2±0.7; p=0.15) (Fig. 3B). Additionally, control tumors had a significantly larger proportion staining positive for vWF (11.2±1.4%) than motesanib-treated tumors (4±0.9%) ($p<0.01$) (Fig. 3C), suggesting that motesanib treatment reduced the number as well as the caliber of vessels coursing through the tumor, with little demonstrable impact on the tumor cell parenchyma. Radiation alone (3 Gy x 8) had a large effect on the tumor parenchyma, reducing the cellular content of tumors. However, vasculature could still be observed throughout the tumor. The combination of motesanib and radiation resulted in the emergence of large necrotic areas within the core of the tumors (Fig. 3A). Similar patterns were demonstrated in SCC-1483 xenografts (data not shown).

Motesanib and radiation impact the tumor microenvironment

To explore the capacity of motesanib to augment antitumor efficacy (Fig. 2) and increase tumor necrosis (Fig. 3) in combination with radiation we examined the intratumoral relationships between tumor vascularity, proliferation, and hypoxia. Mice harboring UM-SCC1 xenografts treated with vehicle control, radiation, motesanib, or the combination (Figure 2A) were injected with pimonidazole HCl (Hypoxyprobe™-1), a validated *in vivo* marker of intracellular hypoxia (14), and harvested 3 hours after the last radiation treatment (day 47, at end of 4^{th} week of treatment). In addition, tumors were stained for markers of vascularity (9F1) and proliferation (Ki67). Vehicle-treated control xenografts showed prominent vessels throughout the tumor, with areas of hypoxia spatially related to the vascular distribution and tumor cell proliferation greatest at the periphery (Fig. 4A). A protracted four week schedule of fractionated radiation was shown to induce higher levels of proliferation (accelerated repopulation), both in the absence of motesanib (2.5-fold increase, p=0.02) and in the presence of motesanib (2.4-fold increase, p=0.04) (Fig 4B). Motesanib alone was not demonstrated to impact tumor cell proliferation.

Treatment with motesanib resulted in a 2-fold increase in hypoxic staining than that observed in control tumors ($p<0.02$) (Fig. 4C). Treatment with radiation (3 Gy x 8) significantly decreased hypoxia in the absence (83% reduction, $p<0.01$) and in the presence of motesanib (70% reduction, $p<0.01$). Furthermore, while radiation treatment lowered levels of hypoxia compared to control, mice treated with motesanib and radiation had significantly higher levels of tumor hypoxia than mice treated with radiation alone (2.5-fold increase, $p<0.01$). Therefore motesanib consistently increased intratumoral hypoxia, both in the presence and absence of fractionated radiation treatment. The impact of motesanib alone on tumor vasculature was not apparent in this small subset (n=3 per group) of xenografts (Fig. 4C).

Discussion

This study presents evidence that motesanib, a potent inhibitor of the VEGF family of receptors, can augment the antitumor efficacy of radiation in tumor xenograft models of HNSCC. To examine mechanisms that may underlie this observed enhancement of radiation effect, we confirm that motesanib shows antiproliferative activity in VEGF-driven endothelial cell models (HUVECs) *in vitro*, both as a sole agent and in combination with radiation. We further confirm that motesanib blocks the VEGF stimulated kinase activity and phosphorylation of VEGFR2. *In vivo*, we examined the effect of motesanib and radiation treatments on tumor histomorphology, and provide evidence that the combination may interact by altering the intratumoral distribution of vasculature, hypoxia, and proliferation.

The interaction between antiangiogenic therapeutic agents and radiation has been extensively studied (7, 8, 10, 15–17). *In vitro*, VEGF (7) and PDGF (10) have been shown to protect against the effects of radiation on endothelial cells, and receptor tyrosine kinase inhibitors of these signaling cascades, as well as VEGFR-specific antibodies, have shown efficacy in abrogating these radioprotective effects *in vitro* (10, 15, 16). We demonstrate that motesanib inhibited VEGF-stimulated HUVEC proliferation and VEGFR2 kinase activity in a dose-dependent fashion (Fig.1). Additionally, in media containing VEGF, motesanib exerted mild antiproliferative activity on HUVECs, and when combined with fractionated radiation more potently inhibited HUVEC proliferation. Furthermore, *in vitro* data suggests that motesanib acts specifically on endothelial cells, as motesanib had no activity on HNSCC cells in either proliferative assays or clonogenic radiation assays.

The interaction between antiangiogenic agents and radiation is most relevant *in vivo*, and remains an area of active investigation in both preclinical models, and in clinical trials involving patients with solid tumors. When initially postulated (18), it was presumed that antiangiogenic agents held potential to limit the supply of oxygen and nutrients to tumors, thereby limiting proliferative potential. However, limiting tumor oxygenation could result in hypoxia-mediated radioresistance; indeed, some studies combining antiangiogenic agents and radiation have shown an antagonistic interaction (19, 20). However, our group (16, 17) and others have shown that antiangiogenic therapy can augment radiation efficacy in various tumor models. While specific mechanisms of these interactions are difficult to isolate, effects on tumor cell repopulation and hypoxia are thought to underlie radiation resistance in HNSCC.

Accelerated repopulation of HNSCC tumors undergoing radiotherapy is a recognized clinical phenomenon that can limit the efficacy of radiotherapy in advanced HNSCC (21). Furthermore, the magnitude of accelerated repopulation during fractionated radiotherapy is thought to peak 3–5 weeks into the course of treatment (22). We performed detailed histomorphologic and immunohistochemical examinations of xenograft tissue after four weeks of fractionated radiation and/or motesanib treatment. By staining for tumor vasculature, we identified that motesanib altered the penetration of vessels into tumor xenografts (Fig. 3), similar to previously published reports (11, 23). We also provide evidence that motesanib treatment results in significantly increased intratumoral hypoxia and that hypoxia is spatially related to tumor vessel distribution (Fig. 4). These findings in motesanib treated xenografts have implications when considering the addition of fractionated radiation as an antitumor agent.

Some of the antitumor effects of radiation are demonstrable when examining tumor tissue microscopically (Fig. 3). Many tumor clonogens are killed by radiation, and subsequently the tumor parenchyma of irradiated xenografts shows reduced cellularity than control tumors

or tumors treated with motesanib alone. However, irradiated tumors demonstrate more Ki67 staining than control xenografts, providing evidence for accelerated repopulation in this model (Fig. 4). When these rapidly proliferating cells were deprived of nutrients and oxygen by combining the antiangiogenic agent motesanib with radiation, we observed smaller tumors (Fig. 2) with increased regions of hypoxia (Fig. 4) and markedly enhanced areas of tumor necrosis (Fig. 3). A recent study in breast cancer xenograft models demonstrated enhanced tumor necrosis after motesanib treatment (23). Radiation, by inducing accelerated proliferative activity of remaining clonogens and thereby increasing cellular oxygen and nutrient demand may effectively prime tumor clonogens for the antitumor effect of motesanib.

A limitation of the current study is that the molecular targets of motesanib were not readily detectable in our tested HNSCC tumor cell lines (supplemental Figure 1) and motesanib did not show demonstrable activity in the HNSCC tumor cell lines *in vitro* (data not shown). These data however do corroborate published reports demonstrating that motesanib effects are mediated by inhibitory effects on endothelial cell signaling. Indeed, Polverino *et al* (11) have shown that motesanib potently inhibits mouse VEGFR2, and provides data demonstrating *in vivo* biologic activity in mouse endothelial models.

The specific clinical implications of the current findings to human cancer patients remain unknown. Motesanib was demonstrated to significantly induce hypoxia in tumor xenografts, and the prevalence of radioresistant cancer stem cells may be upregulated by hypoxia (24). These results suggest that the sequencing of radiation and anti-angiogenic therapies warrant careful clinical evaluation with reports suggesting that radiation followed by anti-angiogenic treatment as the most logical approach (25). Only carefully conducted clinical trials can answer these questions in definitive fashion.

Motesanib is undergoing clinical evaluation in several solid tumor settings and has been demonstrated to be well tolerated in phase I studies with promising early antitumor activity in phase II settings (26, 27). The present studies demonstrate that motesanib can augment radiation response in endothelial cells *in vitro*, and in HNSCC tumor xenograft model systems *in vivo*. These findings suggest that clinical investigations examining the combination of radiation and motesanib are warranted in HNSCC.

Supplementary Material

Refer to Web version on PubMed Central for supplementary material.

Acknowledgments

Work supported in part by laboratory research grant from Amgen Inc. and by National Institutes of Health/National Cancer Institute Grant R01 CA 113448 to PMH. TJK supported by NIH T32 grant (CA009614–17 Physician Scientist Training in Cancer Medicine)

References

1. Jemal A, Siegel R, Ward E, et al. Cancer statistics, 2008. CA Cancer J Clin. 2008; 58:71–96. [PubMed: 18287387]
2. Pignon JP, le Maitre A, Bourhis J. Meta-Analyses of Chemotherapy in Head and Neck Cancer (MACH-NC): an update. Int J Radiat Oncol Biol Phys. 2007; 69:S112–4. [PubMed: 17848275]
3. Bonner JA, Harari PM, Giralt J, et al. Radiotherapy plus cetuximab for squamous-cell carcinoma of the head and neck. N Engl J Med. 2006; 354:567–78. [PubMed: 16467544]

4. Kyzas PA, Stefanou D, Batistatou A, Agnantis NJ. Prognostic significance of VEGF immunohistochemical expression and tumor angiogenesis in head and neck squamous cell carcinoma. J Cancer Res Clin Oncol. 2005; 131:624–30. [PubMed: 16044346]
5. Oc P, Rhys-Evans P, Eccles SA. Expression of vascular endothelial growth factor family members in head and neck squamous cell carcinoma correlates with lymph node metastasis. Cancer. 2001; 92:556–68. [PubMed: 11505400]
6. Tse GM, Chan AW, Yu KH, et al. Strong immunohistochemical expression of vascular endothelial growth factor predicts overall survival in head and neck squamous cell carcinoma. Ann Surg Oncol. 2007; 14:3558–65. [PubMed: 17929099]
7. Gorski DH, Beckett MA, Jaskowiak NT, et al. Blockage of the vascular endothelial growth factor stress response increases the antitumor effects of ionizing radiation. Cancer Res. 1999; 59:3374–8. [PubMed: 10416597]
8. Gupta VK, Jaskowiak NT, Beckett MA, et al. Vascular endothelial growth factor enhances endothelial cell survival and tumor radioresistance. Cancer J. 2002; 8:47–54. [PubMed: 11895203]
9. Bussink J, Kaanders JH, van der Kogel AJ. Microenvironmental transformations by VEGF- and EGF-receptor inhibition and potential implications for responsiveness to radiotherapy. Radiother Oncol. 2007; 82:10–7. [PubMed: 17141899]
10. Timke C, Zieher H, Roth A, et al. Combination of vascular endothelial growth factor receptor/platelet-derived growth factor receptor inhibition markedly improves radiation tumor therapy. Clin Cancer Res. 2008; 14:2210–9. [PubMed: 18381963]
11. Polverino A, Coxon A, Starnes C, et al. AMG 706, an oral, multikinase inhibitor that selectively targets vascular endothelial growth factor, platelet-derived growth factor, and kit receptors, potently inhibits angiogenesis and induces regression in tumor xenografts. Cancer Res. 2006; 66:8715–21. [PubMed: 16951187]
12. Rosen LS, Kurzrock R, Mulay M, et al. Safety, pharmacokinetics, and efficacy of AMG 706, an oral multikinase inhibitor, in patients with advanced solid tumors. J Clin Oncol. 2007; 25:2369–76. [PubMed: 17557949]
13. Rijken PF, Peters JP, Van der Kogel AJ. Quantitative analysis of varying profiles of hypoxia in relation to functional vessels in different human glioma xenograft lines. Radiat Res. 2002; 157:626–32. [PubMed: 12005540]
14. Haustermans K, Hofland I, Van de Pavert L, et al. Diffusion limited hypoxia estimated by vascular image analysis: comparison with pimonidazole staining in human tumors. Radiother Oncol. 2000; 55:325–33. [PubMed: 10869747]
15. Abdollahi A, Lipson KE, Han X, et al. SU5416 and SU6668 attenuate the angiogenic effects of radiation-induced tumor cell growth factor production and amplify the direct anti-endothelial action of radiation in vitro. Cancer Res. 2003; 63:3755–63. [PubMed: 12839971]
16. Li J, Huang S, Armstrong EA, Fowler JF, Harari PM. Angiogenesis and radiation response modulation after vascular endothelial growth factor receptor-2 (VEGFR2) blockade. Int J Radiat Oncol Biol Phys. 2005; 62:1477–85. [PubMed: 16029810]
17. Hoang T, Huang S, Armstrong E, Eickhoff JC, Harari PM. Augmentation of radiation response with the vascular targeting agent ZD6126. Int J Radiat Oncol Biol Phys. 2006; 64:1458–65. [PubMed: 16488554]
18. Folkman J. Tumor angiogenesis: therapeutic implications. N Engl J Med. 1971; 285:1182–6. [PubMed: 4938153]
19. Murata R, Nishimura Y, Hiraoka M. An antiangiogenic agent (TNP-470) inhibited reoxygenation during fractionated radiotherapy of murine mammary carcinoma. Int J Radiat Oncol Biol Phys. 1997; 37:1107–13. [PubMed: 9169820]
20. Wachsberger PR, Burd R, Marero N, et al. Effect of the tumor vascular-damaging agent, ZD6126, on the radioresponse of U87 glioblastoma. Clin Cancer Res. 2005; 11:835–42. [PubMed: 15701874]
21. Bentzen SM. Repopulation in radiation oncology: perspectives of clinical research. Int J Radiat Biol. 2003; 79:581–5. [PubMed: 14530167]

22. Roberts SA, Hendry JH. The delay before onset of accelerated tumour cell repopulation during radiotherapy: a direct maximum-likelihood analysis of a collection of worldwide tumour-control data. Radiother Oncol. 1993; 29:69–74. [PubMed: 8295990]

23. Coxon A, Bush T, Saffran D, et al. Broad antitumor activity in breast cancer xenografts by motesanib, a highly selective, oral inhibitor of vascular endothelial growth factor, platelet-derived growth factor, and Kit receptors. Clin Cancer Res. 2009; 15:110–8. [PubMed: 19118038]

24. Heddleston JM, Li Z, Lathia JD, Bao S, Hjelmeland AB, Rich JN. Hypoxia inducible factors in cancer stem cells. Br J Cancer. 102:789–95. [PubMed: 20104230]

25. Murata R, Siemann DW, Overgaard J, Horsman MR. Improved tumor response by combining radiation and the vascular-damaging drug 5,6-dimethylxanthenone-4-acetic acid. Radiat Res. 2001; 156:503–9. [PubMed: 11604063]

26. Schlumberger MJ, Elisei R, Bastholt L, et al. Phase II study of safety and efficacy of motesanib in patients with progressive or symptomatic, advanced or metastatic medullary thyroid cancer. J Clin Oncol. 2009; 27:3794–801. [PubMed: 19564535]

27. Sherman SI, Wirth LJ, Droz JP, et al. Motesanib diphosphate in progressive differentiated thyroid cancer. N Engl J Med. 2008; 359:31–42. [PubMed: 18596272]

Statement of Translational Relevance

In this study we examine the interaction between radiation and motesanib, a potent, orally bioavailable inhibitor of VEGFR1, 2, and 3, PDGFR and Kit receptors, in xenograft models of head and neck squamous cell carcinoma (HNSCC). The intratumoral interactions between antiangiogenic agents and radiation remain poorly understood, and we demonstrate that motesanib can augment radiation response in HNSCC xenografts. By employing immunohistochemical techniques, low dose radiation schedules are shown to induce accelerated repopulation in this model, and motesanib is found to alter the tumor microenvironment in a way that limits oxygen delivery to radiated xenografts, resulting in tumor necrosis. These findings highlight potential mechanisms of radiosensitization that warrant consideration in future preclinical studies and clinical trial design. Furthermore, the techniques utilized demonstrate that the interplay between tumor vasculature, oxygenation, and clonogenic proliferation can be studied in vivo in response to fractionated radiation with concurrent antiangiogenic therapy.

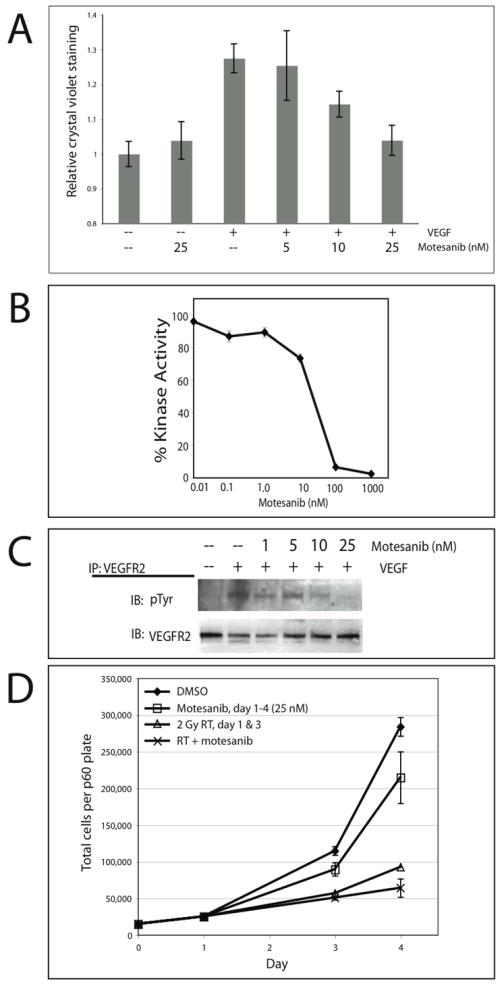

Fig 1.

Motesanib *in vitro* activity on VEGFR2 signaling and interaction with radiation. **(A)** Impact of motesanib on VEGF-stimulated HUVEC proliferation. Cells were grown in EBM-2 basal medium with 2% FBS, without exogenous growth factors. VEGF stimulation was 25 ng/ml every 24 hours x 4 days. Final DMSO concentration was 0.25% in all wells. Data points represent the mean crystal violet staining intensity (6 wells per condition) +/− SEM. **(B)** Motesanib blocks VEGFR2 kinase activity. VEGFR2 kinase activity was determined in presence of serial dilutions of motesanib. **(C)** Motesanib blocks VEGF stimulation of VEGFR2 phosphorylation in HUVECs. HUVECs were pretreated with motesanib for 24 hours, collected after stimulation with 50 ng/ml VEGF x 45 min. IP = immunoprecipitation; IB = immunoblot. **(D)** HUVECs seeded day 0, exposed to motesanib or DMSO days 1–4, and radiated x 2 on days 1 and 3 were harvested and counted via trypan blue exclusion. Points represent mean of 3 plates per condition at days 1, 3, and 4, +/− SEM

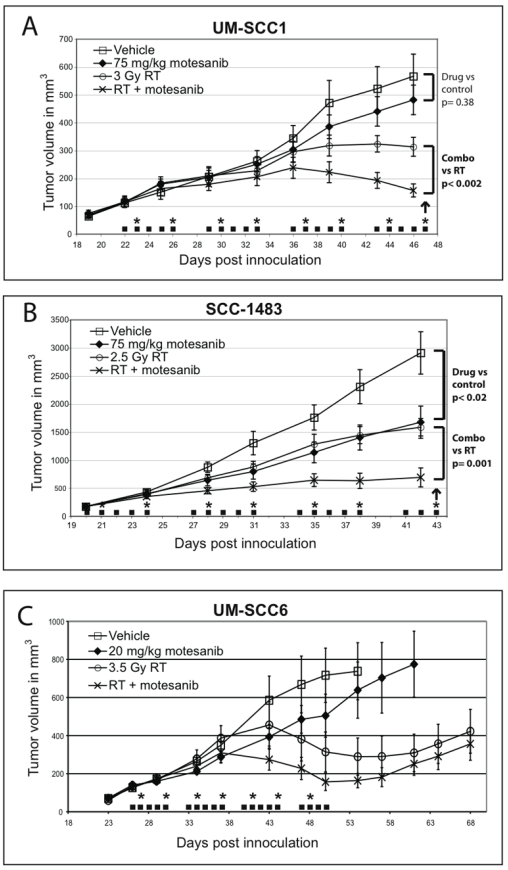

Fig 2.

Motesanib augments radiation response in tumor xenograft models. Mice bearing UM-SCC1 **(A)**, SCC-1483 **(B)**, or UMSCC-6 **(C)** tumors were treated with either motesanib or vehicle by oral gavage 5x weekly (■). Twice weekly radiation was also administered (*). Data points are expressed as mean tumor size (n=10/group) +/− SEM. Arrows represent days that tumors were harvested for immunohistochemistry (as presented in Figures 3 & 4).

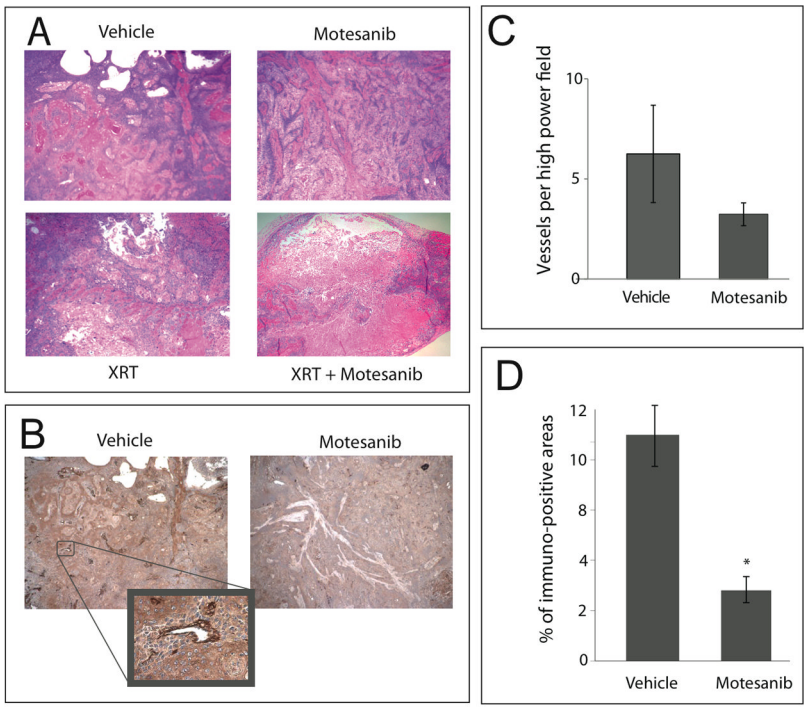

Fig 3.

Vascular distribution and tumor architecture in UM-SCC1 xenografts. Tumors from mice harboring UM-SCC1 xenografts were harvested after 4 weeks of treatment (see Fig. 2 for details). Tumor architecture **(A)** was observed under low power (20x) via H&E staining. **(B)** Tumor tissue was stained for expression of von Willebrand Factor (vWF), which stains tumor vasculature, as demonstrated at 200x (inset). **(C,D)** Quantitative analysis of vWF staining was performed at 100x magnification. Five high-powered fields per tumor were randomly chosen and vessel density was quantified by counting the vessels (C) and examining the percentage of vWF immunoreactive area (D) using Image J software. Control tumors had a significantly larger proportion staining positive for vWF than motesanib-treated tumors (* $p < 0.01$; Students t-test). Data represent mean ± SEM.

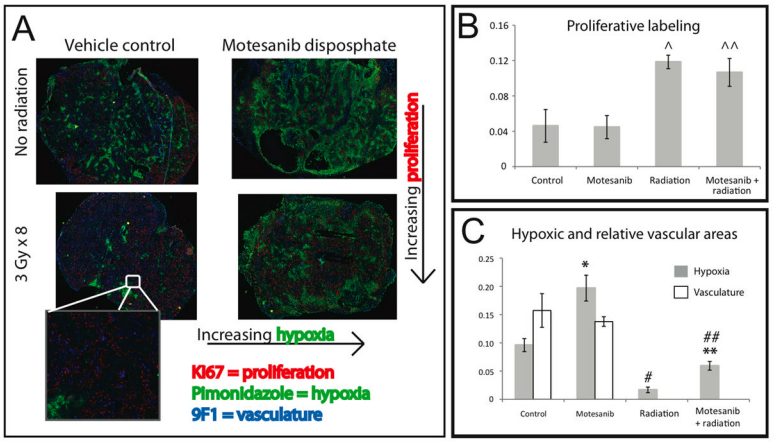

Fig 4.

Impact of motesanib on intratumoral hypoxia (pimonidazole), proliferation (Ki67), and vasculature (9F1). Mice bearing UMSCC-1 xenografts (see Fig. 2 for treatment schema) were inoculated with pimonidazole (PIMO) by intra peritoneal injection 1 hour after the last radiation dose. Tumors were then harvested 2 hours later (3 hours after last radiation dose). Tumor tissue was then analyzed by immunohistochemistry for expression of PIMO, 9F1, and Ki67. Representative tumor sections are shown. **(A)** Tumor hypoxia and proliferation show spatial relationships to tumor vasculature (inset) **(B)** Four weeks of fractionated radiation results in higher levels of proliferative staining (Ki67), both in the absence of motesanib (^; *p=0.02*) and in the presence of motesanib (^^; *p=0.04*) (Fig 4B). Motesanib was not demonstrated to impact tumor cell proliferation. **(C)** Hypoxic staining of each tumor was analyzed, and impact of motesanib on vascular staining was assessed. Treatment with motesanib resulted in significantly more hypoxia in tumors not exposed to fractionated radiation (*; *p <0.02, students t-test*) and tumors exposed to fractionated radiation (**; *p <0.01).* Radiation significantly reduced the hypoxic fraction in tumors in the absence (#; *p <0.01*) and presence (##; p <0.01) of motesanib. The impact of motesanib on tumor vasculature was not apparent in this subset of xenografts Data represent mean ± SEM (n=3 in all groups).